Cerebrovascular disease promotes tau pathology in Alzheimer's disease

Krystal K. Laing[1], Sabrina Simoes[1], Gloria P. Baena-Caldas[2,3], Patrick J. Lao[1], Milankumar Kothiya[1], Kay C. Igwe[1], Anthony G. Chesebro[1], Alexander L. Houck[1], Lina Pedraza[2], A. Iván Hernández[4,7], Jie Li[2], Molly E. Zimmerman[5], José A. Luchsinger[6], Frank C. Barone[2,7], Herman Moreno[2,7], and Adam M. Brickman[1*]

for the Alzheimer's Disease Neuroimaging Initiative**

1. Taub Institute for Research on Alzheimer's Disease and the Aging Brain, G.H. Sergievsky Center, and Department of Neurology, College of Physicians and Surgeons, Columbia University. New York, NY
2. Departments of Neurology and Physiology/Pharmacology. SUNY Downstate. Brooklyn, NY
3. School of Biomedical Sciences, Health Sciences Division, Universidad del Valle, Cali, Colombia.
4. Department of Pathology. SUNY Downstate. Brooklyn, NY
5. Department of Psychology, Fordham University. Bronx, NY.
6. Department of Medicine, College of Physicians and Surgeons. Department of Epidemiology, Joseph P. Mailman School of Public Health. Columbia University.
7. The Robert F. Furchgott Center for Neural and Behavioral Science, Downstate Medical Center, State University of New York, Brooklyn, NY, United States of America

***Corresponding author**
Taub Institute for Research on Alzheimer's Disease and the Aging Brain
P&S Box 16
College of Physicians and Surgeons
Columbia University
630 West 168th Street
New York, NY 10032 USA
Tel: +1 212 342 1348
Fax: +1 212 342 1838
Email: amb2139@columbia.edu

**Data used in preparation of this article were obtained from the Alzheimer's Disease Neuroimaging Initiative (ADNI) database (adni.loni.usc.edu). As such, the investigators within the ADNI contributed to the design and implementation of ADNI and/or provided data but did not participate in analysis or writing of this report.
A complete listing of ADNI investigators can be found at: http://adni.loni.usc.edu/wp-content/uploads/how_to_apply/ADNI_Acknowledgement_List.pdf

Running title: Small vessel cerebrovascular disease and tau

Abstract

Small vessel cerebrovascular disease, visualized as white matter hyperintensities on T2-weighted MRI, contributes to the clinical presentation of Alzheimer's disease. However, the extent to which cerebrovascular disease represents an independent pathognomonic feature of Alzheimer's disease or directly promotes Alzheimer's pathology is unclear. The purpose of this study was to examine the association between white matter hyperintensities and plasma levels of tau and to determine if white matter hyperintensities and tau levels interact to predict Alzheimer's disease diagnosis. To confirm that cerebrovascular disease promotes tau pathology, we examined tau fluid biomarker concentrations and pathology in a mouse model of ischemic injury.

Three hundred ninety-one participants from the Alzheimer's Disease Neuroimaging Initiative (ADNI; 74.5 ± 7.1 years of age) were included in this cross-sectional analysis. Participants had measurements of plasma total-tau, CSF beta amyloid, and white matter hyperintensities, and were diagnosed clinically as Alzheimer's disease (n=97), mild cognitive impairment (n=186), or cognitively normal control (n=108). We tested the relationship between plasma tau concentration and white matter hyperintensity volume across diagnostic groups. We also examined the extent to which white matter hyperintensity volume, plasma tau, amyloid positivity status, and the interaction between white matter hyperintensities and plasma tau correctly classifies diagnostic category. Increased white matter hyperintensity volume was associated with higher plasma tau concentration, particularly among those diagnosed clinically with Alzheimer's disease. Presence of brain amyloid and the interaction between plasma tau and white matter

hyperintensity volume distinguished Alzheimer's disease and mild cognitive impairment participants from controls with 77.6% and 63.3% accuracy, respectively.

In 63 ADNI participants who came to autopsy (82.33 ± 7.18 age at death) we found that higher degrees of arteriosclerosis were associated with higher Braak staging, indicating a positive relationship between cerebrovascular disease and neurofibrillary pathology.

In a transient middle cerebral artery occlusion (tMCAo) mouse model, aged mice that received tMCAo, but not sham surgery, had increased plasma and CSF tau concentrations, induced myelin loss, and hyperphosphorylated tau pathology in the ipsilateral hippocampus and cerebral hemisphere.

These findings demonstrate a relationship between cerebrovascular disease, operationalized as white matter hyperintensities, and tau levels, indexed in the plasma, suggesting that hypoperfusive injury promotes tau pathology. This potential causal association is supported by the demonstration that transient cerebral artery occlusion induces white matter damage, increases biofluidic markers of tau, and promotes cerebral tau hyperphosphorylation in older adult mice.

Keywords: Alzheimer's disease, white matter hyperintensities, tau, cerebrovascular disease, plasma biomarkers

Abbreviations:

AD=Alzheimer's disease
ADNI=Alzheimer's Disease Neuroimaging Initiative
CERAD=Consortium to Establish a Registry for Alzheimer's Disease
CSF=cerebrospinal fluid
CVD=cerebrovascular disease
DAB=3,3′-Diaminobenzidine
ELISA=enzyme-linked immunosorbent assay
MPRAGE=magnetic prepared rapid gradient echo
MRI=magnetic resonance imaging
NC=normal control
NIA-AA=National Institute on Aging-Alzheimer's Association
PBS=phosphate buffered saline
PD=proton density
PET=positron emission tomography

IACUC=institutional animal care and use committee
MBP=myelin basic protein
MCI=mild cognitive impairment
RU=relative units
RUO=research use only
Simoa=single molecule array
tMCAo=transient middle cerebral artery occlusion

Introduction

Models of Alzheimer's disease (AD) pathogenesis emphasize prescribed pathological changes that begin with beta amyloid deposition, tau pathology, and associated neurodegeneration (Jack *et al.*, 2013, 2018). However, in recent years there has been increased appreciation of the contribution of vascular and cerebrovascular disease (CVD) to the clinical expression of AD. Epidemiologic data emphasize vascular factors, such as hypertension, midlife obesity, and diabetes in the increased risk for clinical AD (Barnes and Yaffe, 2011). Neuroimaging and pathological studies highlight that CVD co-occurs with primary AD pathology and drives disease expression more often than not (Schneider *et al.*, 2004; Kapasi *et al.*, 2017). There is also a clear 'shared genetic risk' for CVD and AD with several cardiovascular-associated genes increasing risk for clinical AD (Broce *et al.*, 2018). These studies have generally been interpreted as evidence that CVD is a common comorbidity that contributes additively to the clinical symptoms of AD. However, the question of whether small vessel CVD promotes AD pathology directly remains critical. A primary, pathogenic role of CVD in AD-related pathology and neurodegeneration could help to identify novel disease-modifying therapeutic targets.

Small vessel CVD manifests on magnetic resonance imaging (MRI) T2-weighted sequences as white matter hyperintensities (WMH) (Wardlaw *et al.*, 2015). Joining other studies that implicate WMH in AD (Yoshita *et al.*, 2006; Mimenza-Alvarado *et al.*, 2018), we showed previously that higher WMH volume is associated with increased risk of incident clinical AD (Brickman *et al.*, 2012, 2015), rate of cognitive decline among individuals with AD (Brickman *et al.*, 2008), and the APOE-ε4 allele (Brickman *et al.*, 2014). Individuals with autosomal dominant, fully penetrant forms of AD manifest

increased WMH above non-mutation carrier control participants up to 20 years prior to expected age of clinical onset, establishing WMH as a "core feature" of AD (Lee *et al.*, 2016).

Whether WMH - - or the underlying small vessel ischemic CVD they represent - - cause accumulating AD pathology remains an open question. Most studies show no reliable relationship between WMH or other markers of white matter abnormality and amyloid pathology (Hedden *et al.*, 2012) (cf.(Grimmer *et al.*, 2012)), but emerging animal studies suggest that cerebral hypoperfusion or ischemia do indeed increase tau hyperphosphorylation (p-tau) (Raz *et al.*, 2019), which may be mediated by local inflammatory changes (Jalal *et al.*, 2015). It is difficult to test these types of AD marker associations in humans because cerebrospinal and PET biomarkers are invasive, costly, and difficult to acquire in adequate numbers of participants with MRI data to test hypotheses with sufficient statistical power. However, ultrasensitive ELISA techniques have been developed to assay tau levels in the plasma (Rissin *et al.*, 2010*a*). While generally considered inadequate on its own for diagnostic purposes, there is consensus that plasma tau levels reflect AD-associated cerebral tau pathology because they are elevated among participants with clinical AD compared with unimpaired controls; correlate positively with cerebrospinal tau levels and negatively with amyloid levels; and predict cognition difficulties, cognitive decline, brain atrophy, and decreasing cortical glucose metabolism (Mattsson *et al.*, 2016; Pase *et al.*, 2019). There are other compelling reasons to consider plasma measures when examining the association between cerebrovascular and AD makers. Plasma tau measures relate specifically to markers of small vessel CVD examined at autopsy, including microinfarcts (Pase *et al.*, 2019).

Compared with central markers of tau pathology, plasma total tau measures may also most accurately reflect damage related to ischemia induced blood brain barrier breakdown, which would allow smaller fragments of tau protein to pass into the blood than what remains in the parenchyma or CSF (Fossati *et al.*, 2019).

Here, we tested the hypothesis that increased WMH volume is associated with increased tau pathology, indexed by plasma levels, in the Alzheimer's Disease Neuroimaging Initiative (ADNI). A second hypothesis was that the strength of the relationship between WMH and tau levels increases as a function of clinical diagnostic category (i.e., normal control (NC), mild cognitive impairment (MCI) and clinical AD), reflecting the possibility that small vessel disease drives tau pathology, which has a subsequent impact on cognition and function. We further examined the extent to which WMH severity and its interaction with tau pathology predicts clinical diagnosis. Additionally, in order to determine whether the observations of an association between WMH and plasma tau measures suggests a relationship between small vessel cerebrovascular disease and tau pathology, we examined the correlation between severity of arteriosclerosis and neurofibrillary tangle pathology in a group of participants who came to autopsy.

To confirm a causal effect of CVD on tau pathology, we used a well-established rodent model of transient occlusion with reperfusion (Barone *et al.*, 2009, 2012) and determined if brain ischemia-reperfusion causes white matter damage, increased plasma and CSF tau concentrations, and cerebral tau hyperphosphorylation. This model produces myelin damage that mediates aspects of cognitive decline in animal models (Zhou *et al.*, 2013; Liu *et al.*, 2018). The etiology of WMH is likely heterogeneous, and factors that have been implicated consistently include ischemia, hypoxic damage, and/or hypoperfusion

(Wardlaw *et al.*, 2015). We thus consider this model, particularly when implemented in older mice, as a relevant approach that can be used to test the hypothesis that small vessel CVD induces tau pathology. When combined with the human data, the present mouse studies provide initial experimental evidence that brain ischemia, reflected in humans as WMH, induces tau pathology that is independent of beta amyloid.

Materials and Methods

Alzheimer's Disease Neuroimaging Initiative (ADNI)

Human data used in the preparation of this article were obtained through the ADNI database (www.adni.loni.usc.edu), which was launched in 2003 as a public-private partnership and is led by Principal Investigator Michael W. Weiner, MD. The primary goal of ADNI has been to test whether serial MRI, PET, other biological markers, and clinical and neuropsychological assessments can be analyzed and related to measures of the progression from normal control to MCI and early AD dementia. All participating institutions received appropriate ethical approval from corresponding institutional review boards and ethics committees. Written informed consent was obtained from all study participants involved, or their legal surrogates. Up-to-date information is available at www.adni-info.org.

Participants

We used ADNI data accessed on June 22, 2018. The study data and samples were collected from September 7, 2005, to September 18, 2007. Data were obtained for all participants classified as cognitively healthy controls, having MCI, or having AD dementia. Inclusion in the current study was limited to participants who also had available baseline derived plasma levels of tau and CSF measures of $A\beta_{42}$ (n=391).

General ADNI exclusion criteria included significant vascular disease risk history, defined as a Modified Hachinski Ischemia scale greater than 4. Recruitment and diagnostic procedures were described previously (Petersen, 2010). Characteristics and demographics for participants in this study are included in Table 1. Neuropathological data were obtained for 63 ADNI participants, 27 of whom were included in the antemortem analyses.

Neuroimaging Acquisition

A standardized MRI protocol was validated and implemented across ADNI sites (Jack *et al.*, 2008*a*). High-resolution T1-weighted volumetric magnetization prepared rapid gradient echo (MPRAGE) sequences were obtained in the sagittal orientation on 1.5T MRI systems. An axial proton density (PD)/T2-weighted dual contrast fast spin echo sequence was also acquired for detection of WMH (Jack *et al.*, 2008a). All sites were required to pass a rigorous scanner validation and each subject scan acquisition included fluid-filled phantoms. Details of scan validations can be found on the ADNI site (www.adni.loni.usc.edu).

White Matter Hyperintensity Quantification / Volumetric Data

Detailed WMH quantification methods have been provided previously (Schwarz *et al.*, 2009). Briefly, T1-, T2- and PD-weighted MRI scans were co-registered, brain extracted, and corrected for bias field inhomogeneity (Decarli *et al.*, 1996; Wolz *et al.*, 2011). White matter hyperintensities were detected at each voxel based on the corresponding T1, T2, and PD intensities, the prior probability of WMH, and the conditional probability of WMH based on the presence of WMH in neighboring voxels. Total WMH volumes were derived by summing voxels identified as hyperintense (Schwarz *et al.*, 2009). White

matter hyperintensity volumes derived at the ADNI baseline visit were included in this study.

In addition to WMH volume, cerebral volumetric data were downloaded from ADNI. Volumetric data were derived with FreeSurfer (http://surfer.nmr.mgh.harvard.edu/; (Dale and Sereno, 1993; Dale *et al.*, 1999, Fischl *et al.*, 1999*a*, *a*, *b*, 2001, 2002, 2004; Han *et al.*, 2006; Jovicich *et al.*, 2006; Ségonne *et al.*, 2007) applied to T1-weighted volumetric MRI. We calculated relative total volume (total brain volume/total intracranial volume) and relative white matter volume (total white matter volume/intracranial volume) as indicators of total brain and total white matter atrophy, respectively.

Human Cerebrospinal Fluid Biomarkers

Cerebrospinal fluid (CSF) samples were collected at study baseline using the microbead-based multiplex immunoassay INNO-BIA AlzBio3 research use only (RUO) test (Fujirebio, Ghent, Belgium) and run on the Luminex platform (Shaw *et al.*, 2009). Detailed methods of the validation study, assay technology and quality measurements are located on the ADNI site (www.adni.loni.usc.edu). Due to the variation in reagent lot kit measured concentrations, typical in RUO immunoassay tests, multiple batch runs were acquired per participant. The median values provided by ADNI, which average the values obtained from the multiple reagent lot kits, were used for the analyses reported here. The CSF samples were drawn at baseline assessment, but the analytical run was conducted on March 9, 2016. CSF measures of $A\beta_{42}$ were used to determine amyloid positivity, which was derived from the cut off value of 192 pg/ml (Shaw *et al.*, 2011). Cerebrospinal fluid measures of total tau and phosphorylated tau were also obtained and used as secondary outcomes.

Human Plasma Tau Measurements

Plasma tau measurements were obtained at baseline and analyzed with the Quanterix "Single molecule Array" (Simoa) HD1 analyzer and Human Total Tau kit, using a monoclonal antibody capture that responded to a linear epitope in all tau isoforms. Detailed methods and analyses have been described in previous publications (Mattsson *et al.*, 2016, Rissin *et al.*, 2010*b*; Randall *et al.*, 2013). Further information on quantification can be found on the ADNI site (www.adni.loni.usc.edu).

Neuropathology Validation

To examine whether observed relationships between WMH and plasma tau suggest a relationship between small vessel disease and tau pathology, we turned to neuropathological data collected in ADNI. The ADNI neuropathology protocol follows National Institute on Aging-Alzheimer's Association (NIA-AA) guidelines for assessment of AD (Montine *et al.*, 2012). Using standardized neuropathological outcomes derived from the NIA-AA protocol, an "ABC" score for neuropathological change was generated by ADNI to include histopathologic assessments of amyloid β deposits using Thal phases (A), Braak staging of neurofibrillary degeneration (B), and CERAD scoring of neuritic plaques (C), in addition to detailed methods of assessing co-morbid conditions such as vascular brain injury (Montine *et al.*, 2012). We calculated a summary arteriosclerosis index, comprising the sum of scalar arteriosclerosis severity ratings (absent/none = '0', mild = '1', moderate = '2', severe = '3') across 23 brain regions, including middle frontal gyrus, anterior cingulate gyrus, precentral gyrus, superior and middle temporal gyri, inferior parietal lobe, occipital lobe, amygdala, entorhinal cortex, CA1, dentate gyrus, parahippocampal gyrus, atherosclerosis within the

circle of Willis and arteriosclerosis in various subcortical regions. We examined the relationship between the summary arteriosclerosis index and neurofibrillary pathology, operationally-defined as overall Braak staging. Further information on post-mortem quantification procedures and brain regions sampled can be found on the ADNI site (www.adni.loni.usc.edu/methods/neuropath-methods/).

Mouse Ischemia-Reperfusion Model

Mouse use was carried out in strict accordance with the recommendations in the Guide for the Care and Use of Laboratory Animals of the National Institutes of Health (National Research Council (US) Committee for the Update of the Guide for the Care and Use of Laboratory Animals, 2011). Reporting the data on these mice follows the Animal Research: Reporting In Vivo Experiments (ARRIVE) guidelines for animal research (Kilkenny *et al.*, 2011). The experimental and surgical protocol for this research was approved by the SUNY Downstate Institutional Animal Care and Use Committee (IACUC) under Protocol Number 15-10475. All surgery was done under deep isoflurane anesthesia. Euthanasia was performed under deep isoflurane anesthesia using exsanguination and whole-body perfusion. All efforts were made to minimize or eliminate animal suffering.

In order to confirm that cerebral hypoperfusion, a source of WMH, can induce tau pathology, we used a well-established 30- and 60-min transient middle cerebral artery occlusion (tMCAo) brain ischemia-reperfusion model in mice. We performed tMCAo in older-adult mice (13.72±3.67-months-old) in order to phenocopy the human condition more closely. The tMCAo procedure or sham surgery (Barone *et al.*, 2012) was conducted on 13 female C57Bl/6 J (Jackson Labs; Bar Harbor, ME) mice, grouping

chosen at random, with 8 receiving tMCAo (30 min, n=4; 60 min, n=4) and 5 receiving Sham surgery. Briefly, under 2% isoflurane anesthesia, a monofilament suture (6.0, from Doccol Corp, Sharon, MA) was inserted through the proximal external carotid artery, advanced into the internal carotid artery and positioned to occlude the origin of MCA (about 10 mm from the common carotid artery bifurcation). Mice recovered from anesthesia, and after 30 or 60 min of occlusion they were re-anesthetized with isoflurane and the intraluminal filament was withdrawn to allow reperfusion. Most tMCAo protocols in mice and rats use occlusion times of 60 min or 120 min followed by reperfusion to produce relatively consistent brain infarctions that affect about 30% of the cerebral hemisphere. Infarcted brain areas include somatosensory, motor, and parietal cortices and the striatum (Zhou *et al.*, 2011, 2013; Barone *et al.*, 2012). Here, we used 30 minute and 60 min tMCAo to evaluate a range of hypoperfusion injury and to better approximate the variable ischemic damage seen in human WMH. Sham surgery animals were subjected to the same procedure, but without occlusion-reperfusion of the MCA. Body temperature was continuously maintained at 37.0 ± 0.5°C using the Heat Therapy Pump-1500 and Temperature Therapy Pad (Adroit Medical Systems, Louden, TN, USA) until animals recovered completely from anesthesia. Animals were then placed in their home cages, monitored closely over the next 4 hours and then daily for the rest of the study. Body weight was monitored throughout the experiments and changed minimally (<5%) due to surgery.

Perfusion and Fixation

The animals were perfused as previously described (Hernández *et al.*, 2014). Briefly, mice were perfused with PBS followed by 4% PFA/PBS. The brains were harvested and

post-fixed in PFA/PBS and transferred to 30% sucrose in PBS until the brains were isopycnic with the solution. The brains were then quickly frozen in n-methylbutane, cooled over dry ice, and kept at -80^{o}C for cryostat sectioning. Free-floating coronal brain sections (30 μm) were obtained with coordinates between -1.34 and -1.46 posterior to Bregma and immunostained as described below.

Immunohistochemistry

We harvested the mouse brains 12-15 days after surgery for immunohistochemical and immunofluorescence analysis of myelin basic protein, total-tau, and p-tau.

Light Microscopy. These methods have been described previously (Hernández *et al.*, 2014; Gutiérrez-Vargas *et al.*, 2017). In short after quenching, sections were washed with PBS and incubated with the phospho-tau (Ser 202, Thr 205; {1:500}) monoclonal antibody (AT8; Invitrogen, Waltham, USA), anti-tau antibody (Tau5 {1:250} Abcam, Cambridge, USA,). Tau5 is a pan-tau antibody that labels monomeric and aggregated tau equally well (Carmel *et al.*, 1996). AT8 recognizes phosphorylated tau in mouse and human (Biernat *et al.*, 1992). Tauopathy in AD is usually staged with AT8 antibodies (Braak *et al.*, 2006). Sections were then incubated with biotinylated secondary antibody (1:2000) washed and then incubated with Vectastain (Vector Laboratories, Burlington, Canada), followed by DAB (ImmPACT, Vector Laboratories), which was used to stain sections for light microscopy examination. Immunostaining intensity was evaluated with image J (NIH, Bethesda, MD). The images were converted to a binary system, and integrated densities (relative units, RU) were obtained for each image. The background was automatically subtracted from each image to quantify the relative intensity of the

immunostaining. For details see (Nguyen and Nguyen, 2013; Gutiérrez-Vargas *et al.*, 2017)

Immunofluorescence Microscopy. For immunofluorescence AT8 (1:500) and myelin basic protein (MBP; 1:2000 polyclonal antibody, Invitrogen) were incubated overnight, followed by the secondary antibodies that included Alexa Fluor® 488 conjugated Goat anti-mouse (1:1000) and Alexa Fluor 647-conjugated Goat anti-chicken (1:200; both from Abcam). Sections were mounted on glass slides with DAPI solution (Vectashield, from Vector laboratories). Omission of the primary antibodies resulted in no staining. The sections were photographed at 40X magnification and the images were used to evaluate the fluorescence intensity (FI) of MBP immunostaining in regions of interest (ROIs) located in the corpus callosum and stratum alveus. Images were obtained using the laser Olympus FV 1000D microscope and IF was measure with Fluoview FV1000 software. P-tau was evaluated by calculating the total number cells immuno-stained with signal larger than 8 microns. All analyses were performed per mouse and for each mouse 3 slides were measured (Nguyen and Nguyen, 2013).

As tMCAo can cause changes in the posterior circulation as well (Lee *et al.*, 2014), we examined the hippocampal formation and the ipsilateral hemisphere.

Cerebrospinal Fluid (CSF) and Plasma Collection in Mice

Cerebrospinal fluid and plasma samples were collected from anesthetized animals 15 days after tMCAo and Sham surgeries and prior to transcardial perfusion. Mice were anesthetized via intraperitoneal injection with a mixture containing ketamine (100 mg/kg body weight) and xylazine (10 mg/kg body weight). For CSF samples, anesthetized mice were placed in a prone position and the skin covering the back of the neck was shaved. A

cotton swab containing 70% ethanol was used to remove any hair from the exposed skin. Then, a 27-gauge sterile needle (SV*27EL, Terumo Medical Products) attached to a 1-ml syringe (329650, BD Biosciences) was inserted into the cisterna magna allowing flow of CSF into the butterfly needle. After 10-15 secs, the needle was removed and the CSF aspirated into microcentrifuge tubes (1605-0000, USA Scientific), followed by a brief centrifugation at 600xg for 6 mins at 4°C. Supernatant was transferred to a new tube, immediately placed on dry ice, and further stored at -80°C. Roughly 5-10uL of fluid was collected per mouse. Cerebrospinal fluid visibly contaminated with blood (pelleted residual erythrocytes) was discarded. All remaining samples underwent more stringent assessment for blood contamination via hemoglobin ELISA (cat# ab157715, Abcam) using 0.5uL CSF with a 1:200 dilution. Samples below 0.01% blood contamination were used for tau quantitation.

For plasma samples, whole blood collected from the submandibular vein was directly poured into anticoagulant EDTA-treated tubes. Animals were restrained with one-hand technique and a lancet (5mm) was used to puncture the submandibular vein. Samples were centrifuged at 2000xg for 15 min at 4°C. The supernatant was transferred to a new tube, immediately frozen in liquid nitrogen, and further stored at -80°C.

Cerebrospinal Fluid and Plasma Tau Quantitation in Mice

Cerebrospinal fluid and plasma tau were quantified by Simoa technology using the murine total-tau assay (cat# 102209, Quanterix). Individual CSF and plasma samples were diluted in sample buffer at 1:75 and 1:4, respectively, and then split into technical duplicates (100ul/ replicate). Standards and samples were run according to the manufacturer's instructions and read on the SR-X analyzer (Quanterix).

Statistical Analysis

Demographic data, including age and sex, and biomarker data, including percentage of individuals classified as amyloid positive, plasma tau levels, and total WMH volume, were compared across the three diagnostic groups (NC, MCI, and AD) with analysis of variance for continuous variables and Chi-squared analysis for proportional data. For primary hypothesis testing, we used a mixed design general linear model that included diagnostic group, amyloid status (negative, positive), plasma tau levels, the interaction between diagnostic group and plasma tau levels, and the interaction between amyloid status and plasma tau levels as primary predictors of total WMH volume. Mean centered participant age was included in the model as a covariate. In the case of interactions, the data were stratified by the categorical variable (e.g., diagnostic group) and multiple regression analysis was used to test associations within group. We hypothesized that increased plasma tau levels would be associated with increased WMH volume, and that this relationship would be stronger across diagnostic groups (NC <MCI< AD). This model was repeated with CSF-derived measures of total tau and phosphorylated tau.

To test the possibility that observed effects involving WMH volume reflect associations with AD-related neurodegeneration in general (and not changes related to ischemia per se), we re-ran the mixed design general linear model designed to test the primary hypothesis with relative total brain volume and relative white matter volume as dependent variables. We then repeated the primary analysis adjusting for relative total brain volume.

We used a series of binary logistic regression analyses to examine the extent to which amyloid positivity, plasma tau levels, WMH volume, and the interaction between WMH

volume and tau levels could classify participants into diagnostic groups. We ran separate analyses that contrasted AD participants to controls, AD participants to MCI participants, and MCI participants to controls; these analyses included mean-centered age as an additional covariate.

For post-mortem neuropathology validation, we performed a regression analysis, adjusting for age at death, to examine the relationship between the arteriosclerosis index and neurofibrillary tangle pathology.

In mice, plasma and CSF tau concentrations were compared between tMCAo mice and Sham controls with general linear models. We examined the relationship between plasma and CSF derived concentrations with Pearson correlations. Similarly, RU and IF signals, reflecting tau and MBP levels, obtained from 3 slides per mouse were compared between tMCAo and sham mice with general linear models.

Data Availability

ADNI data are available to the general scientific community through online request (http://adni.loni.usc.edu/data-samples/access-data/).

Results

Human Data

Table 1 displays demographic and biomarker data for ADNI participants across the three diagnostic groups. The three groups were similar in age and sex distribution. Amyloid positivity and plasma tau levels varied reliably across groups in the expected direction: a greater proportion of individuals diagnosed with AD were classified as amyloid positive

compared with those diagnosed with MCI, who in turn, were more likely to be amyloid positive than controls. Plasma tau levels increased monotonically across the three diagnostic groups.

Results from the primary mixed design general linear model that examined the relationship of plasma tau concentrations and WMH across diagnoses showed a trend for increasing WMH volume across diagnostic groups ($F_{(2,382)}$=2.98, p=0.05; see Figure 1). Increased plasma tau concentrations were associated with higher WMH volume (main effect of plasma tau, $F_{(1,382)}$=5.27, p=0.022, B=0.743 [0.259, 1.228]; see Figure 2) and this relationship differed across diagnostic groups (diagnostic group by plasma tau interaction, $F_{(2,382)}$=4.95, p=0.008). The analysis stratified by diagnostic group confirmed that the magnitude of the relationship between plasma tau levels and WMH volume increased across the diagnostic groups and was strongest among participants diagnosed with AD (NC: B=-0.083[-0.34-0.17], MCI: B=0.038[-0.15-0.22], AD: B=0.448 [0.16-0.72]; see Figure 3). Neither amyloid positivity ($F_{(1,382)}$1.32, p=0.25) nor the amyloid positivity by tau plasma concentration interaction ($F_{(1,382)}$=2.16, p=0.14) was associated with WMH volume. Older age was associated with greater WMH volume ($F_{(1,382)}$=12.09, p=0.03, B=0.050 [0.022-0.079]). When the analyses were repeated with CSF total tau and phosphorylated tau rather than plasma levels, there was a trend for a positive association between WMH and the CSF tau measures ($F_{(1,382)}$=1.67, p=0.19 and $F_{(1,382)}$=2.93, p=0.09 for main effects of total and p-tau, respectively), but these relationships did not vary as a function of diagnostic group ($F_{(2,382)}$=0.37, p=0.68 and $F_{(2,382)}$=0.19, p=0.82 for total tau and p-tau by diagnostic group interactions, respectively).

Plasma tau levels were not related to relative total brain volume as a main effect ($F_{(1,382)}$=0.731, p=0.39) or interacting with diagnosis ($F_{(2,382)}$=1.31, p=0.27) nor were they related to relative white matter volume as a main effect ($F_{(1,382)}$=0.255, p=0.61) or interacting with diagnosis ($F_{(2,382)}$=0.221, p=0.80). When we re-ran the primary analysis, above, adjusting for relative total volume, we found the main effect of plasma tau ($F_{(1,381)}$=6.26, p=0.01) and the interaction between plasma tau levels and diagnosis ($F_{(2,381)}$=4.72, p=0.009) to be of similar or even greater magnitude.

Results of the logistic regression analyses that examined whether the biomarkers discriminate among diagnostic groups are presented in Table 2. In the analysis discriminating participants diagnosed with AD from controls, 77.6% of participants were correctly classified (χ^2=88.91, p<0.001, sensitivity, 89.7%; specificity, 66.7%). Amyloid positivity was highly associated with an increased likelihood of being diagnosed with clinical AD. In this model, increased WMH volume was associated with a lower likelihood of being diagnosed with clinical AD, and plasma tau levels were not associated with diagnosis (i.e., main effects of WMH volume and plasma tau levels). However, without the interaction term in the model, WMH volume trended positively with AD classification. That is, including an interaction term with plasma tau (B=0.49*tau) in the model (Table 2), the main effect of WMH on diagnosis was negative (B=-1.18), but the total effect of WMH (B= -1.18 + 0.49*tau) becomes positive at higher levels of plasma tau (above tau of 2.41, B > -1.18 + 0.49*2.41 > 0). Therefore, the total effect of WMH predicts that higher WMH volume, at higher levels of plasma tau, is associated with a greater likelihood of being AD over NC. Plasma tau levels and WMH interacted to increase likelihood of AD diagnosis, such that that individuals with increased WMH

volume were particularly likely to be classified as clinical AD when tau levels were also elevated. Very similar results were observed in the analysis that discriminated MCI participants form controls (χ^2=45.99, p<0.001, 63.3% correctly classified (sensitivity, 78.0%; specificity: 61.1%,)); that is, increased amyloid, decreased WMH volume, and the interaction between plasma tau levels and WMH volume were associated with greater likelihood of MCI diagnosis. In the analysis discriminating AD participants from those with MCI (χ^2=21.807, p=0.001, 66.1% correctly classified (sensitivity, 4.1%; specificity: 98.4%), only amyloid positivity was associated with an increased likelihood for diagnosis of AD.

Next, we turned to neuropathological data to confirm the association we observed between WMH and plasma tau concentration reflects a relationship between small vessel disease and tau pathology. Demographic data and descriptive neuropathological data for the autopsy sample are displayed Table 3. When examining the postmortem data, we observed a positive relationship between arteriosclerosis severity and neurofibrillary tangle severity (B=0.06, F= 4.21, p=0.04).

Mouse Model Data

We turned to a mouse tMCAo model to confirm the correlations observed in human data and to test whether induced hypoperfusion causes ischemic injury to white matter and associated tau pathology. Hypoperfusion via tMCAo produced focal infarct and widespread white matter ischemic damage, based on myelin basic protein (MBP) immunofluorescence (IF) staining analysis. Mice exposed to 60 min tMCAo had lower IF MBP signal in the corpus collosum (307.41+/- 41), followed by mice exposed to the 30 min tMCAo (357.11+/- 42.3), and then Sham controls (428.5+/-27;$F_{(1,5)}$ =18.05, p=0.01).

Similarly, IF MBP values were lower in the alveus of the CA1 subregion of tMCAo mice, with 60 min (283.2+/-44.1), 30 min (355+/- 73.12) and Sham (451.6 +/- 93.08; $F_{(1,5)}$=8.08, p=0.04; see Figures 4 and 5).

Using immunohistological analysis, we further observed that although Tau5 (pan - tau) immunoreactivity in the hippocampal regions did not differ greatly between 30 or 60 min tMCAo conditions (27.44 +/-7.5 RU vs. 27.88+/-1.9 RU), there was greater reactivity observed in both tMCAo groups than in Sham mice (20.52+/- 0.4; $F_{(2,12)}$=4.575 p=0.02); formal post hoc testing showed, relative to Sham mice, a trend increase in the 30 min condition (p=0.05) and a significant increase in the 60 min condition (p=0.03; focal changes in staining can be seen Figure 6) . In addition, the pattern of staining produced by AT8 showed accumulation of abnormal phosphorylated tau in the CA3 region of the ipsilateral hippocampus in tMCAo compared with sham mice, which was particularly prominent in 60 min tMCAo mice (60.53+/-1.6 RU) but also in 30min tMCAo mice (47.43+/-3.03 RU) when compared with Sham controls (22.8+/- 1.4 RU; $F_{(2,12)}$=26.8 p=0.0001; post hoc testing showed reliable increases in both conditions (p=0.0001) relative to Sham (see Figure 6). Similarly, immunofluorescence signal for AT8 evaluating cells labeled with signal > 8 μm in stratum pyramidal CA1 was highest in 60 min tMCAo mice (47.17 +/- 7.2), followed by 30 min tMCAo mice (31.2+/-19) and Sham mice (12.33+/-6.7; $F_{(1,5)}$=18,21p=0.004; see Figure 4).

Next, we investigated if tau changes observed in the brains of tMCAo animals and suggested by the human data, followed the exact same trend in CSF and plasma biofluids. For this purpose, Simoa technology was used for tau measurements, as described in Methods. Figure 7 shows tMCAo-associated differences in plasma and CSF tau levels

across tMCAo and Sham groups. Cerebrospinal fluid and plasma total tau levels were elevated among mice following 60 min tMCAo (mean± SD= 339.55+/- 136.08 pg/ml; mean± SD= 183.34+/- 53.82 pg/ml, respectively) compared with mice following 30 min tMCAo (mean± SD= 107.98+/- 10.92 pg/ml; mean± SD= 50.37+/- 42.56 pg/ml, respectively) and Sham controls (mean± SD= 138.37+/- 61.93 pg/ml; mean± SD= 80.77+/- 26.81 pg/ml, respectively; $F_{(2,11)}$=7.38, p=0.013 for CSF tau and $F_{(2,11)}$=10.70, p=0.004 for plasma tau). Furthermore, plasma and CSF tau measurements were highly correlated with each other (R^2=0.522, β=0.36, p=0.008).

Discussion

White matter hyperintensities are considered a radiological marker of small vessel CVD due to regional hypoperfusion (Wardlaw *et al.*, 2013) and have been implicated in the clinical expression of AD (Brickman *et al.*, 2015). Here we demonstrate a direct relationship between increased WMH volume and plasma total tau levels, particularly among individuals diagnosed clinically with AD, suggesting the effect of small vessel CVD on risk and expression of AD is due partially to its promotion of tau pathology. The interaction between WMH and tau, independent of amyloid pathology, was associated with an increased likelihood of clinical AD and MCI, and postmortem markers of small vessel cerebrovascular disease were associated with severity of neurofibrillary pathology. Results from the human experiment are consistent with an emerging literature highlighting a tau pathway for AD pathogenesis that is independent of beta amyloid pathology (Weigand *et al.*, 2020); our findings suggest that cerebrovascular abnormalities may be one initiator of this pathway. The results from the human studies confirm a relationship between markers of tau and WMH of presumed vascular origin.

The conceptual model we were testing was based on the hypothesis that ischemia or hypoperfusion damage that manifests radiologically as WMH causes or promotes AD-related tau pathology independent of beta amyloid. Our previous work showed that baseline measures of WMH predict longitudinal increases in CSF tau, but not vice versa (Tosto *et al.*, 2015), and recent studies show that forebrain hypoperfusion that occurs in hypoxia-ischemia induced white matter injury is associated with increased phosphorylated tau levels in rats (Raz *et al.*, 2019). Because cross-sectional analyses with human biomarker or postmortem data indicate co-dependency but not necessarily causality, we used a tMCAo mouse model to test the possibility that hypoperfusion results in white matter damage and can indeed induce tau pathology. Findings from this mouse model demonstrate that cerebral hypoperfusion results in decreased myelin (i.e., white matter ischemic damage) and increased tau pathology, providing experimental support for the correlational analyses in humans and for our conceptual model. Only total-tau levels were available in the human data and previous work suggests that although total-tau levels are also elevated in the context of AD, phosphorylated tau plasma levels may be a more specific marker (Mielke *et al.*, 2018); thus the observation of a clear relationship between induced hypoperfusion in mice and distributed *phosphorylated* tau levels provides evidence of a specific relationship between cerebrovascular injury and AD pathology. The abnormal tau phosphorylation observed following tMCAo mirrors what is seen in human AD. That is, the diagnostic antibody AT8 is specific to tau phosphorylation site S202/205, as seen in tauopathies such as AD (Braak *et al.*, 2006). Further, in addition to observing increased tau phosphorylation throughout the ipsilateral occluded hemisphere, there was dramatically increased tau

change in the ipsilateral hippocampal formation, where earliest tau-related changes are observed in human AD (de Calignon *et al.*, 2012). Of note, in control mice we did not observe robust tau signal in corpus callosum analyzed (Figure 6), which is likely due to the anterior location of the sections sampled, where normal tau is marginally seen compared with more medial or posterior sections and because normal tau has stronger labeling in non-myelinated than in myelinated axons (Kubo *et al.*, 2019). We also performed identical Simoa-based measurements in mice and humans and confirmed increased CSF and plasma markers of tau pathology, as we observed in humans. We believe this study is among the first to consider Simoa-derived plasma tau biomarkers in murine models. Another unique aspect of our study is that, while most tMCAo studies use young-adult mice, in the present work, mice were aged to create a phenocopy more closely related to the human condition. Histological and biofluidic evidence of tau pathology in our study was more robust in the 60 min tMCAo condition than in the 30 min condition, suggesting a "dose effect" of ischemia on these markers. Our human-to-mouse study establishes the biological plausibility that ischemia, known to manifest radiologically in humans as WMH, can indeed induce an AD-like tauopathy independent of beta amyloid.

Together with others (Raz *et al.*, 2019), our findings do not preclude the concomitant possibility that some degree of white matter damage *results* from tau-related neurodegeneration in a Wallerian-like fashion, a hypothesis tested by at least two other groups (McAleese *et al.*, 2017; Graff-Radford *et al.*, 2019). In one study (McAleese *et al.*, 2017), cortical tau pathology, but not markers of CVD, correlated with white matter abnormalities in autopsied brain tissue derived from participants with AD, suggesting a

neurodegenerative rather than a vascular source of the white matter changes. We suspect that in end stage AD (i.e., at autopsy), in addition to parenchymal degeneration, there is degeneration of the small vessels, which may obscure relationships between vessel pathology and white matter abnormalities earlier in the disease in some autopsy series. In the current study, however, we confirmed that at postmortem markers of vessel disease (arteriosclerosis) are associated with neurofibrillary tangles. We additionally tested this possibility by adjusting for markers of degeneration (relative brain volume) and demonstrating that a reliable association between WMH and tau markers persists. The extant literature further highlights how midlife measures of hypertensive blood pressure are associated with postmortem markers of AD pathology alluding to chronic effects of hypoperfusion (Petrovitch *et al.*, 2000), and that both ante-mortem and post-mortem MRI-derived white matter abnormalities correlate with neurofibrillary pathology (Polvikoski *et al.*, 2010; Brickman *et al.*, 2018). Graff-Radford and colleagues (Graff-Radford *et al.*, 2019) showed no spatial or severity relationship between WMH volume and cortical tau pathology on PET among community-dwelling older adults without dementia. Our findings of a lack of relationship between WMH and tau levels among individuals without dementia parallel these observations; in our analyses, the relationship was most prominent among symptomatic individuals, suggesting that ischemic damage is driving some degree of tau pathology among those with impairment or that there is a critical threshold of ischemic damage required to induce tau pathology and associated cognitive impairment. Finally, there is the possibility that the relationship between tau pathology and vascular abnormalities in humans may be bidirectional, as a recent study

(Bennett *et al.*, 2018) demonstrated there are morphological changes to blood vessels and increases in blood vessel density with the overexpression of tau.

According to current pathogenic theories of AD (Jack *et al.*, 2013), tau accumulation with accompanying neurodegeneration and cognitive impairment comprises the final pathway to AD dementia. This study joins previous efforts in demonstrating an amyloid-independent effect of vascular abnormalities on this pathway; a recent study (Kim *et al.*, 2018), for example, demonstrated that the relationship between small vessel CVD and cognitive status is mediated in part by tau pathology in the medial temporal lobe among patients with subcortical vascular impairment. These findings have both important theoretical and clinical implications. From a theoretical perspective, the possibility that small vessel CVD should be considered a core pathological feature of AD needs to be entertained, not simply because it confers additive risk to the clinical expression of the disease, but because it directly affects primary AD pathology. In this vein, the extent to which AD is diagnosed based on a single pathogenic pathway (Jack *et al.*, 2018) should be questioned. From a clinical perspective, prevention of or intervention on vascular risk factors and CVD may have a direct effect on tau-related neurodegeneration and dementia and/or mitigate the pernicious effects of amyloid pathology.

Although previous studies demonstrated that cerebral hypoperfusion and ischemia promote hyperphosphorylation of tau (Raz *et al.*, 2019), the mechanisms linking the two are poorly understood. Compelling work with spontaneously hypertensive/stroke prone rats showed increased blood brain barrier dysfunction following unilateral carotid artery occlusion, which in turn promoted neuroinflammatory white matter injury (Jalal *et al.*, 2015). Similarly, in chronic hypertensive rats with induced hypoperfusion injury, there

was white matter injury and an increase in endogenous phosphorylated tau coupled with increase in free radicals and active interleukin-1β (Raz *et al.*, 2019). An increase in inflammatory microglia and the sensitivity of white matter mature and immature oligodendrocytes/precursors to ischemia plays a role in white matter injury and associated cognitive decline in transient occlusion models (Nasrabady *et al.*, 2018). Thus, we hypothesize that increased white matter injury due to ischemia/hypoperfusion induces tau pathology via an inflammatory cascade. It is important to emphasize that this pathway is likely independent of amyloid pathology and points to hypoperfusion and inflammatory changes as potential targets for intervention or prevention.

We used a plasma-derived biomarker for total tau pathology, which has advantages and disadvantages. Plasma total tau tracks well with disease progression and is correlated reasonably well with central markers of tau derived from CSF and cognitive decline, but seems to operate independent of amyloid pathology (Mielke *et al.*, 2017) and not considered accurate enough for diagnostic purposes (Mattsson *et al.*, 2016). Plasma-derived markers of the phospho-tau181 isoform, however, may be more sensitive and specific to amyloid pathology than total tau (Mielke *et al.*, 2018; Janelidze *et al.*, 2020; Thijssen *et al.*, 2020). When we examined CSF tau measures, our observations were in a similar direction but less statistically reliable, raising questions about whether the impact of cerebrovascular disease on tau biomarkers differs between CSF and blood markers. It is possible that neurons and/or glia within regions that are most affected by hypoperfusion are also more accessible to plasma membrane translocation, resulting in a higher concentration of tau secretion through plasma membrane (Brunello *et al.*, 2019). Future studies will need to understand the factors that increase tau levels in the blood

versus CSF. Only total tau concentrations were available to us in the current study. With evidence of elevated measures of phosphorylated-tau as a direct response to hypoperfusion in our mouse model, our findings contribute to the growing suspicion of a compounding pathology, suggesting that hypoperfusion induces white matter abnormalities that affect tau hyperphosphorylation. To further elucidate the relationship between hypoperfusion and tau elevation in AD, future studies will need to confirm that plasma-derived measures of phosphorylated tau are associated with markers of small vessel cerebral vascular disease.

In summary, our work suggests a codependency between WMH of presumed vascular origin and tau, which increases with clinical diagnosis of AD. We confirmed the biological plausibility that hypoperfusion-ischemia induces tau pathology in a transient occlusion adult-mouse model. Future studies should focus on better understanding of the causal relationships among cerebrovascular disease, inflammation, and AD pathology in man and mouse.

Acknowledgements

Correspondence: Adam M. Brickman, PhD, Taub Institute for Research on Alzheimer's Disease and the Aging Brain, Department of Neurology, College of Physicians and Surgeons, Columbia University, 630 West 168th St, P&S Box 16, New York, NY 10032 (amb2139@columbia.edu).

Group Information: A list of the Alzheimer's Disease Neuroimaging Initiative Investigators is provided at http://adni.loni.usc.edu/wp-content/uploads/how_to_apply/ADNI_Authorship_List.pdf.

Funding

Data collection and sharing for this project was funded by the Alzheimer's Disease Neuroimaging Initiative (ADNI) (National Institutes of Health grant U01 AG024904) and Department of Defense ADNI (award number W81XWH-12-2-0012). The ADNI is funded by the National Institute on Aging and the National Institute of Biomedical Imaging and Bioengineering, as well as through generous contributions from the following: Alzheimer's Association; Alzheimer's Drug Discovery Foundation; BioClinica Inc; Biogen Idec Inc; Bristol-Myers Squibb Co; Eisai Inc; Elan Pharmaceuticals Inc; Eli Lilly and Co; F. Hoffmann–La Roche Ltd and its affiliated company Genentech Inc; GE Healthcare; Innogenetics NV; IXICO Ltd; Janssen Alzheimer Immunotherapy Research & Development LLC; Johnson & Johnson Pharmaceutical Research & Development LLC; Medpace Inc; Merck & Co Inc; Meso Scale Diagnostics LLC; NeuroRx Research; Novartis Pharmaceuticals Corp; Pfizer Inc; Piramal Imaging; Servier; Synarc Inc; and Takeda Pharmaceutical Co. The Canadian Institutes of Health Research is providing funds to support ADNI clinical sites in Canada. Private-sector contributions are facilitated by the Foundation for the National Institutes of Health (www.fnih.org). The grantee organization is the Northern California Institute for Research and Education, and the study is coordinated by the Alzheimer's Disease Cooperative Study at the University of California–San Diego. The ADNI data are disseminated by the Laboratory for Neuro Imaging at the University of Southern California.

This work was also supported by grants RF1 AG051556 and K24AG045334 from the National Institutes of Health.

Competing Interests

The authors report no competing interests.

References

Barnes DE, Yaffe K. The projected effect of risk factor reduction on Alzheimer's disease prevalence. Lancet Neurol 2011; 10: 819–28.

Barone FC, Rosenbaum DM, Li J, Zhou J, Wang X. Animal Models of Ischemic Stroke: Issues in Translational Congruency. In: Translational Animal Models in Drug Discovery and Development. Bentham Science Publishers; 2012. p. 42–66

Barone FC, Rosenbaum DM, Zhou J, Crystal H. Vascular cognitive impairment: dementia biology and translational animal models. Curr Opin Investig Drugs Lond Engl 2000 2009; 10: 624–37.

Bennett RE, Robbins AB, Hu M, Cao X, Betensky RA, Clark T, et al. Tau induces blood vessel abnormalities and angiogenesis-related gene expression in P301L transgenic mice and human Alzheimer's disease. Proc Natl Acad Sci 2018; 115: E1289–98.

Biernat J, Mandelkow EM, Schröter C, Lichtenberg-Kraag B, Steiner B, Berling B, et al. The switch of tau protein to an Alzheimer-like state includes the phosphorylation of two serine-proline motifs upstream of the microtubule binding region. EMBO J 1992; 11: 1593–7.

Braak H, Alafuzoff I, Arzberger T, Kretzschmar H, Del Tredici K. Staging of Alzheimer disease-associated neurofibrillary pathology using paraffin sections and immunocytochemistry. Acta Neuropathol (Berl) 2006; 112: 389–404.

Brickman AM, Honig LS, Scarmeas N, Tatarina O, Sanders L, Albert MS, et al. Measuring cerebral atrophy and white matter hyperintensity burden to predict the rate of cognitive decline in Alzheimer disease. Arch Neurol 2008; 65: 1202–8.

Brickman AM, Provenzano FA, Muraskin J, Manly JJ, Blum S, Apa Z, et al. Regional White Matter Hyperintensity Volume, Not Hippocampal Atrophy, Predicts Incident Alzheimer Disease in the Community. Arch Neurol 2012; 69: 1621.

Brickman AM, Schupf N, Manly JJ, Stern Y, Luchsinger JA, Provenzano FA, et al. APOE-ε4 and risk for Alzheimer's disease: Do regionally distributed white matter hyperintensities play a role? Alzheimers Dement J Alzheimers Assoc 2014; 10: 619–29.

Brickman AM, Tosto G, Gutierrez J, Andrews H, Gu Y, Narkhede A, et al. An MRI measure of degenerative and cerebrovascular pathology in Alzheimer disease. Neurology 2018; 91: e1402–12.

Brickman AM, Zahodne LB, Guzman VA, Narkhede A, Meier IB, Griffith EY, et al. Reconsidering harbingers of dementia: progression of parietal lobe white matter hyperintensities predicts Alzheimer's disease incidence. Neurobiol Aging 2015; 36: 27–32.

Broce IJ, Tan CH, Fan CC, Jansen I, Savage JE, Witoelar A, et al. Dissecting the genetic relationship between cardiovascular risk factors and Alzheimer's disease. Acta Neuropathol (Berl) 2018

Brunello CA, Merezhko M, Uronen R-L, Huttunen HJ. Mechanisms of secretion and spreading of pathological tau protein [Internet]. Cell Mol Life Sci 2019[cited 2020 Apr 13] Available from: https://doi.org/10.1007/s00018-019-03349-1

de Calignon A, Polydoro M, Suárez-Calvet M, William C, Adamowicz DH, Kopeikina KJ, et al. Propagation of tau pathology in a model of early Alzheimer's disease. Neuron 2012; 73: 685–97.

Carmel G, Mager EM, Binder LI, Kuret J. The Structural Basis of Monoclonal Antibody Alz50's Selectivity for Alzheimer's Disease Pathology. J Biol Chem 1996; 271: 32789–95.

Dale AM, Fischl B, Sereno MI. Cortical surface-based analysis. I. Segmentation and surface reconstruction. NeuroImage 1999; 9: 179–94.

Dale AM, Sereno MI. Improved Localizadon of Cortical Activity by Combining EEG and MEG with MRI Cortical Surface Reconstruction: A Linear Approach. J Cogn Neurosci 1993; 5: 162–76.

Decarli C, Murphy DGM, Teichberg D, Campbell G, Sobering GS. Local histogram correction of MRI spatially dependent image pixel intensity nonuniformity. J Magn Reson Imaging 1996; 6: 519–28.

Fischl B, Liu A, Dale AM. Automated manifold surgery: constructing geometrically accurate and topologically correct models of the human cerebral cortex. IEEE Trans Med Imaging 2001; 20: 70–80.

Fischl B, Salat DH, Busa E, Albert M, Dieterich M, Haselgrove C, et al. Whole brain segmentation: automated labeling of neuroanatomical structures in the human brain. Neuron 2002; 33: 341–55.

Fischl B, Salat DH, van der Kouwe AJW, Makris N, Ségonne F, Quinn BT, et al. Sequence-independent segmentation of magnetic resonance images. NeuroImage 2004; 23 Suppl 1: S69-84.

Fischl B, Sereno MI, Dale AM. Cortical surface-based analysis. II: Inflation, flattening, and a surface-based coordinate system. NeuroImage 1999; 9: 195–207.

Fischl B, Sereno MI, Tootell RB, Dale AM. High-resolution intersubject averaging and a coordinate system for the cortical surface. Hum Brain Mapp 1999; 8: 272–84.

Fossati S, Ramos Cejudo J, Debure L, Pirraglia E, Sone JY, Li Y, et al. Plasma tau complements CSF tau and P-tau in the diagnosis of Alzheimer's disease. Alzheimers Dement Diagn Assess Dis Monit 2019; 11: 483–92.

Graff-Radford J, Arenaza-Urquijo EM, Knopman DS, Schwarz CG, Brown RD, Rabinstein AA, et al. White matter hyperintensities: relationship to amyloid and tau burden [Internet]. Brain 2019[cited 2019 Jun 28] Available from: https://academic.oup.com/brain/advance-article/doi/10.1093/brain/awz162/5519094

Grimmer T, Faust M, Auer F, Alexopoulos P, Förstl H, Henriksen G, et al. White matter hyperintensities predict amyloid increase in Alzheimer's disease. Neurobiol Aging 2012; 33: 2766–73.

Gutiérrez-Vargas JA, Moreno H, Cardona-Gómez GP. Targeting CDK5 post-stroke provides long-term neuroprotection and rescues synaptic plasticity. J Cereb Blood Flow Metab 2017; 37: 2208–23.

Han X, Jovicich J, Salat D, van der Kouwe A, Quinn B, Czanner S, et al. Reliability of MRI-derived measurements of human cerebral cortical thickness: the effects of field strength, scanner upgrade and manufacturer. NeuroImage 2006; 32: 180–94.

Hedden T, Mormino EC, Amariglio RE, Younger AP, Schultz AP, Becker JA, et al. Cognitive Profile of Amyloid Burden and White Matter Hyperintensities in Cognitively Normal Older Adults. J Neurosci 2012; 32: 16233–42.

Hernández AI, Oxberry WC, Crary JF, Mirra SS, Sacktor TC. Cellular and subcellular localization of PKMζ [Internet]. Philos Trans R Soc B Biol Sci 2014; 369[cited 2020 Apr 13] Available from: https://www.ncbi.nlm.nih.gov/pmc/articles/PMC3843872/

Jack CR, Bennett DA, Blennow K, Carrillo MC, Dunn B, Haeberlein SB, et al. NIA-AA Research Framework: Toward a biological definition of Alzheimer's disease. Alzheimers Dement 2018; 14: 535–62.

Jack CR, Bernstein MA, Fox NC, Thompson P, Alexander G, Harvey D, et al. The Alzheimer's Disease Neuroimaging Initiative (ADNI): MRI Methods. J Magn Reson Imaging JMRI 2008; 27: 685–91.

Jack CR, Knopman DS, Jagust WJ, Petersen RC, Weiner MW, Aisen PS, et al. Tracking pathophysiological processes in Alzheimer's disease: an updated hypothetical model of dynamic biomarkers. Lancet Neurol 2013; 12: 207–16.

Jalal FY, Yang Y, Thompson JF, Roitbak T, Rosenberg GA. Hypoxia-induced neuroinflammatory white-matter injury reduced by minocycline in SHR/SP. J Cereb Blood Flow Metab 2015; 35: 1145.

Janelidze S, Mattsson N, Palmqvist S, Smith R, Beach TG, Serrano GE, et al. Plasma P-tau181 in Alzheimer's disease: relationship to other biomarkers, differential diagnosis, neuropathology and longitudinal progression to Alzheimer's dementia. Nat Med 2020; 26: 379–86.

Jovicich J, Czanner S, Greve D, Haley E, van der Kouwe A, Gollub R, et al. Reliability in multi-site structural MRI studies: effects of gradient non-linearity correction on phantom and human data. NeuroImage 2006; 30: 436–43.

Kapasi A, DeCarli C, Schneider JA. Impact of multiple pathologies on the threshold for clinically overt dementia. Acta Neuropathol (Berl) 2017; 134: 171–86.

Kilkenny C, Browne W, Cuthill IC, Emerson M, Altman DG. Animal research: reporting in vivo experiments—The ARRIVE Guidelines. J Cereb Blood Flow Metab 2011; 31: 991–3.

Kim HJ, Park S, Cho H, Jang YK, San Lee J, Jang H, et al. Assessment of Extent and Role of Tau in Subcortical Vascular Cognitive Impairment Using 18F-AV1451 Positron Emission Tomography Imaging. JAMA Neurol 2018; 75: 999–1007.

Kubo A, Misonou H, Matsuyama M, Nomori A, Wada-Kakuda S, Takashima A, et al. Distribution of endogenous normal tau in the mouse brain. J Comp Neurol 2019; 527: 985–98.

Lee S, HONG Y, PARK S, LEE S-R, CHANG K-T, HONG Y. Comparison of Surgical Methods of Transient Middle Cerebral Artery Occlusion between Rats and Mice. J Vet Med Sci 2014; 76: 1555–61.

Lee S, Viqar F, Zimmerman ME, Narkhede A, Tosto G, Benzinger TLS, et al. White matter hyperintensities are a core feature of Alzheimer's disease: Evidence from the dominantly inherited Alzheimer network. Ann Neurol 2016; 79: 929–39.

Liu L-Q, Liu X-R, Zhao J-Y, Yan F, Wang R-L, Wen S-H, et al. Brain-selective mild hypothermia promotes long-term white matter integrity after ischemic stroke in mice. CNS Neurosci Ther 2018; 24: 1275–85.

Mattsson N, Zetterberg H, Janelidze S, Insel PS, Andreasson U, Stomrud E, et al. Plasma tau in Alzheimer disease. Neurology 2016; 87: 1827–35.

McAleese KE, Walker L, Graham S, Moya ELJ, Johnson M, Erskine D, et al. Parietal white matter lesions in Alzheimer's disease are associated with cortical neurodegenerative pathology, but not with small vessel disease. Acta Neuropathol (Berl) 2017; 134: 459–73.

Mielke MM, Hagen CE, Wennberg AMV, Airey DC, Savica R, Knopman DS, et al. Association of Plasma Total Tau Level With Cognitive Decline and Risk of Mild

Cognitive Impairment or Dementia in the Mayo Clinic Study on Aging. JAMA Neurol 2017; 74: 1073–80.

Mielke MM, Hagen CE, Xu J, Chai X, Vemuri P, Lowe VJ, et al. Plasma phospho-tau181 increases with Alzheimer's disease clinical severity and is associated with tau- and amyloid-positron emission tomography. Alzheimers Dement J Alzheimers Assoc 2018; 14: 989–97.

Mimenza-Alvarado A, Aguilar-Navarro SG, Yeverino-Castro S, Mendoza-Franco C, Ávila-Funes JA, Román GC. Neuroimaging Characteristics of Small-Vessel Disease in Older Adults with Normal Cognition, Mild Cognitive Impairment, and Alzheimer Disease. Dement Geriatr Cogn Disord EXTRA 2018; 8: 199–206.

Montine TJ, Phelps CH, Beach TG, Bigio EH, Cairns NJ, Dickson DW, et al. National Institute on Aging-Alzheimer's Association guidelines for the neuropathologic assessment of Alzheimer's disease: a practical approach. Acta Neuropathol (Berl) 2012; 123: 1–11.

Nasrabady SE, Rizvi B, Goldman JE, Brickman AM. White matter changes in Alzheimer's disease: a focus on myelin and oligodendrocytes. Acta Neuropathol Commun 2018; 6: 22.

National Research Council (US) Committee for the Update of the Guide for the Care and Use of Laboratory Animals. Guide for the Care and Use of Laboratory Animals [Internet]. 8th ed. Washington (DC): National Academies Press (US); 2011[cited 2019 Jun 28] Available from: http://www.ncbi.nlm.nih.gov/books/NBK54050/

Nguyen D, Nguyen D. Quantifying chromogen intensity in immunohistochemistry via reciprocal intensity. [Internet]. Protoc Exch 2013[cited 2020 Apr 29] Available from: http://www.nature.com/protocolexchange/protocols/2931

Pase MP, Beiser AS, Himali JJ, Satizabal CL, Aparicio HJ, DeCarli C, et al. Assessment of Plasma Total Tau Level as a Predictive Biomarker for Dementia and Related Endophenotypes [Internet]. JAMA Neurol 2019[cited 2019 Mar 21] Available from: https://jamanetwork.com/journals/jamaneurology/fullarticle/2726948

Petrovitch H, White LR, Izmirilian G, Ross GW, Havlik RJ, Markesbery W, et al. Midlife blood pressure and neuritic plaques, neurofibrillary tangles, and brain weight at death: the HAAS. Honolulu-Asia aging Study. Neurobiol Aging 2000; 21: 57–62.

Polvikoski TM, van Straaten ECW, Barkhof F, Sulkava R, Aronen HJ, Niinistö L, et al. Frontal lobe white matter hyperintensities and neurofibrillary pathology in the oldest old. Neurology 2010; 75: 2071–8.

Randall J, Mörtberg E, Provuncher GK, Fournier DR, Duffy DC, Rubertsson S, et al. Tau proteins in serum predict neurological outcome after hypoxic brain injury from cardiac arrest: Results of a pilot study. Resuscitation 2013; 84: 351–6.

Raz L, Bhaskar K, Weaver J, Marini S, Zhang Q, Thompson JF, et al. Hypoxia promotes tau hyperphosphorylation with associated neuropathology in vascular dysfunction. Neurobiol Dis 2019; 126: 124–36.

Rissin DM, Kan CW, Campbell TG, Howes SC, Fournier DR, Song L, et al. Single-molecule enzyme-linked immunosorbent assay detects serum proteins at subfemtomolar concentrations. Nat Biotechnol 2010; 28: 595–9.

Rissin DM, Kan CW, Campbell TG, Howes SC, Fournier DR, Song L, et al. Single-molecule enzyme-linked immunosorbent assay detects serum proteins at subfemtomolar concentrations. Nat Biotechnol 2010; 28: 595–9.

Schneider JA, Wilson RS, Bienias JL, Evans DA, Bennett DA. Cerebral infarctions and the likelihood of dementia from Alzheimer disease pathology. Neurology 2004; 62: 1148–55.

Schwarz C, Fletcher E, DeCarli C, Carmichael O. Fully-Automated White Matter Hyperintensity Detection With Anatomical Prior Knowledge and Without FLAIR. Inf Process Med Imaging Proc Conf 2009; 21: 239–51.

Ségonne F, Pacheco J, Fischl B. Geometrically accurate topology-correction of cortical surfaces using nonseparating loops. IEEE Trans Med Imaging 2007; 26: 518–29.

Shaw LM, Vanderstichele H, Knapik-Czajka M, Clark CM, Aisen PS, Petersen RC, et al. Cerebrospinal Fluid Biomarker Signature in Alzheimer's Disease Neuroimaging Initiative Subjects. Ann Neurol 2009; 65: 403–13.

Shaw LM, Vanderstichele H, Knapik-Czajka M, Figurski M, Coart E, Blennow K, et al. Qualification of the analytical and clinical performance of CSF biomarker analyses in ADNI. Acta Neuropathol (Berl) 2011; 121: 597–609.

Thijssen EH, Joie RL, Wolf A, Strom A, Wang P, Iaccarino L, et al. Diagnostic value of plasma phosphorylated tau181 in Alzheimer's disease and frontotemporal lobar degeneration. Nat Med 2020; 26: 387–97.

Tosto G, Zimmerman ME, Hamilton JL, T.Carmichael O, Brickman AM. The effect of white matter hyperintensities on neurodegeneration in mild cognitive impairment. Alzheimers Dement J Alzheimers Assoc 2015; 11: 1510–9.

Wardlaw JM, Smith EE, Biessels GJ, Cordonnier C, Fazekas F, Frayne R, et al. Neuroimaging standards for research into small vessel disease and its contribution to ageing and neurodegeneration. Lancet Neurol 2013; 12: 822–38.

Wardlaw JM, Valdés Hernández MC, Muñoz-Maniega S. What are White Matter Hyperintensities Made of? [Internet]. J Am Heart Assoc Cardiovasc Cerebrovasc Dis 2015; 4[cited 2019 Jan 18] Available from: https://www.ncbi.nlm.nih.gov/pmc/articles/PMC4599520/

Weigand AJ, Bangen KJ, Thomas KR, Delano-Wood L, Gilbert PE, Brickman AM, et al. Is tau in the absence of amyloid on the Alzheimer's continuum?: A study of discordant PET positivity [Internet]. Brain Commun 2020; 2[cited 2020 Mar 24] Available from: https://www.ncbi.nlm.nih.gov/pmc/articles/PMC7001143/

Wolz R, Julkunen V, Koikkalainen J, Niskanen E, Zhang DP, Rueckert D, et al. Multi-Method Analysis of MRI Images in Early Diagnostics of Alzheimer's Disease [Internet]. PLoS ONE 2011; 6[cited 2018 Sep 14] Available from: https://www.ncbi.nlm.nih.gov/pmc/articles/PMC3192759/

Yoshita M, Fletcher E, Harvey D, Ortega M, Martinez O, Mungas DM, et al. Extent and distribution of white matter hyperintensities in normal aging, MCI, and AD. Neurology 2006; 67: 2192–8.

Zhou J, Li J, Rosenbaum DM, Barone FC. Thrombopoietin protects the brain and improves sensorimotor functions: reduction of stroke-induced MMP-9 upregulation and blood–brain barrier injury. J Cereb Blood Flow Metab 2011; 31: 924–33.

Zhou J, Zhuang J, Li J, Ooi E, Bloom J, Poon C, et al. Long-Term Post-Stroke Changes Include Myelin Loss, Specific Deficits in Sensory and Motor Behaviors and Complex Cognitive Impairment Detected Using Active Place Avoidance. PLOS ONE 2013; 8: e57503.

Figures Legends

Figure 1. White matter hyperintensity (WMH) volume increases across diagnostic groups. Results from the primary mixed design general linear model shows increasing WMH volume across clinical diagnostic groups. Midline represents the median, the box denotes the 25th percentile and 75th percentile, T-bars represent 95% confidence intervals, points and asterisks represent outliers and extreme outliers, respectively. Y-axis was transformed logarithmically (base10) for visualization. NC = normal control; MCI = Mild Cognitive Impairment; AD = Alzheimer's Disease.

Figure 2. Linear association between white matter hyperintensities (WMH) and plasma tau. Main effect of predicted WMH plotted against predicted plasma tau values obtained from the primary mixed design general linear model ($F_{(1,382)}$=5.27, p=0.022, r^2 =0.153, β=0.743 (95% CI: 0.259-1.228)).

Figure 3. Interaction of WMH and plasma tau levels across diagnostic groups. Stratification across diagnostic groups demonstrate interactions between white matter hyperintensities and plasma tau burden at different diagnostic stages. Participants with Alzheimer's disease had the strongest association (NC: β=-0.083 (95% CI:-0.340-0.175), MCI: β=0.038 (95% CI: -0.152-0.229), AD: r^2=0.677, β=0.448 (95% CI: 0.168-0.728)).

Figure 4. Transient middle cerebral artery occlusion (tMCAo) produces myelin basic protein (MBP) signal loss and induces tau phosphorylation. Representative microphotographs of MBP and AT8 immunofluorescence in mice without stroke (sham, A and D), tMCAo for 30 min (B and E) and 60 min (C and F). tMCAo produced a reduction of MBP (red signal; see arrows in C and F) and induced tau phosphorylation tau (AT8; green signal; see arrows in C, F and inset in F). The degree of ischemia-induced myelin loss and phosphorylation of tau increased with the increasing duration of ischemia (tMCAo) from 30 to 60 min. Panels A-C shows double immunofluorescence (MBP and AT8) with DAPI and panel D-F without DAPI. p, stratum pyramidal CA1; o, stratum oriens of CA1; a, alveus of CA1; corpus callosum. Scale bar = 50μm.

Figure 5. Mice subjected to transient middle cerebral artery occlusion (tMCAo) followed by 15 days reperfusion show strong alterations in the pattern and expression of myelin basic protein (MBP) in corpus callosum and CA1 region of the hippocampus. Shown are three examples of mice subjected to 60 min occlusion surgery (A-C;), which demonstrate a drastic change in MBP expression compared to sham surgery controls (D-F). In addition, tMCAo affects the MBP distribution pattern (compare A-C to D-F). These results suggest myelin loss and axonal damage due to ischemia-reperfusion that is still observed after 15 days. MBP colormap intensity pseudocolor-scale, red is the highest intensity and blue the lowest. cc, corpus callosum; a, alveus; o, stratum oriens; p, stratum pyramidale. Each panel represents an independent mouse (A-C; n=3 and D-F; n=3). Scale bar = 50μm.

Figure 6. Mice undergoing transient middle cerebral artery occlusion (tMCAo) for thirty and sixty minutes followed by 15 days reperfusion exhibit higher total and phosphorylated tau immunostaining in the hippocampus and corpus callosum. Depicted here are representative images of total (Tau-5) and phosphorylated (AT8) tau immunostaining in the CA3 (A-C) and CA1 hippocampal subregions that includes white matter (alveus and corpus callosum areas) (D-F). Thirty minutes tMCAo produced a minor increase in Tau-5 and significant changes in AT8 staining in the stratum oriens (see asterisks in B and E) and corpus callosum (see arrows in E) compared to Sham (non-ischemia surgery A&D) control. Sixty minutes tMCAo showed a greater increase of phosphorylated tau (AT8) immunostaining in pyramidal cells layer of CA3 (arrowheads in C) in addition to significant high intensity of total tau (Tau-5) in the CA1 pyramidal cell layer and in the corpus callosum (see arrowheads and arrows in F). WM, white matter; p, stratum pyramidale; o, stratum oriens; r, stratum radiatum; a, alveus; cc; corpus callosum. Scale bar = 100μm.

Figure 7. Cerebrospinal fluid and plasma tau concentrations differ between mice exposed to tMCAo and sham controls.

A CSF and **B** plasma tau concentrations were particularly pronounced for 60 min tMCAo ($F_{(2,11)}$=7.38, p=0.013 and $F_{(2,11)}$=10.70, p=0.004, respectively). Data are expressed as mean ± S.E.M. **C** Plasma and CSF values were strongly correlated (R^2=0.522, β=0.36, p=0.008). n=7 (Sham), n=2 (tMCAo 30 min), and n=3 (tMCAo 60 min). 60 minute condition displayed in red, 30 minute condition displayed in grey, and sham controls in white.

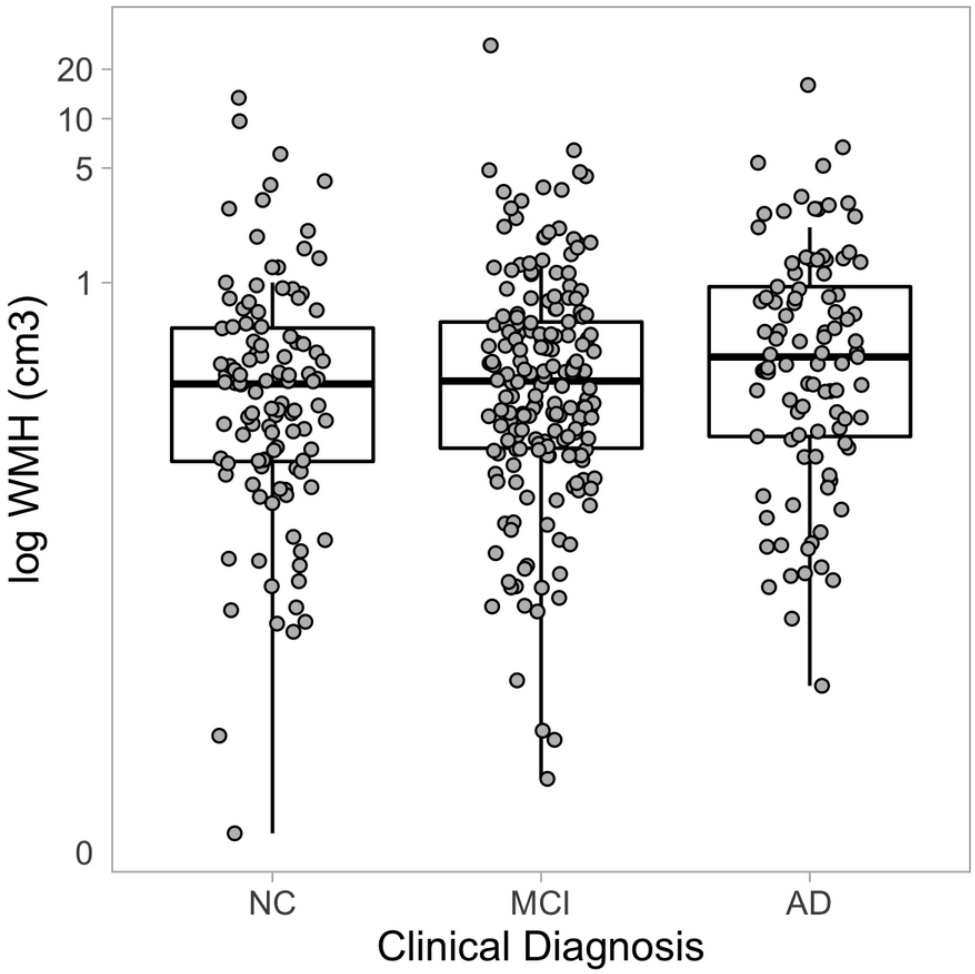

Figure 1. White matter hyperintensity (WMH) volume increases across diagnostic groups. Results from the primary mixed design general linear model shows increasing WMH volume across clinical diagnostic groups. Midline represents the median, the box denotes the 25th percentile and 75th percentile, T-bars represent 95% confidence intervals, points and asterisks represent outliers and extreme outliers, respectively. Y-axis was transformed logarithmically (base10) for visualization. NC = normal control; MCI = Mild Cognitive Impairment; AD = Alzheimer's Disease.

38x38mm (600 x 600 DPI)

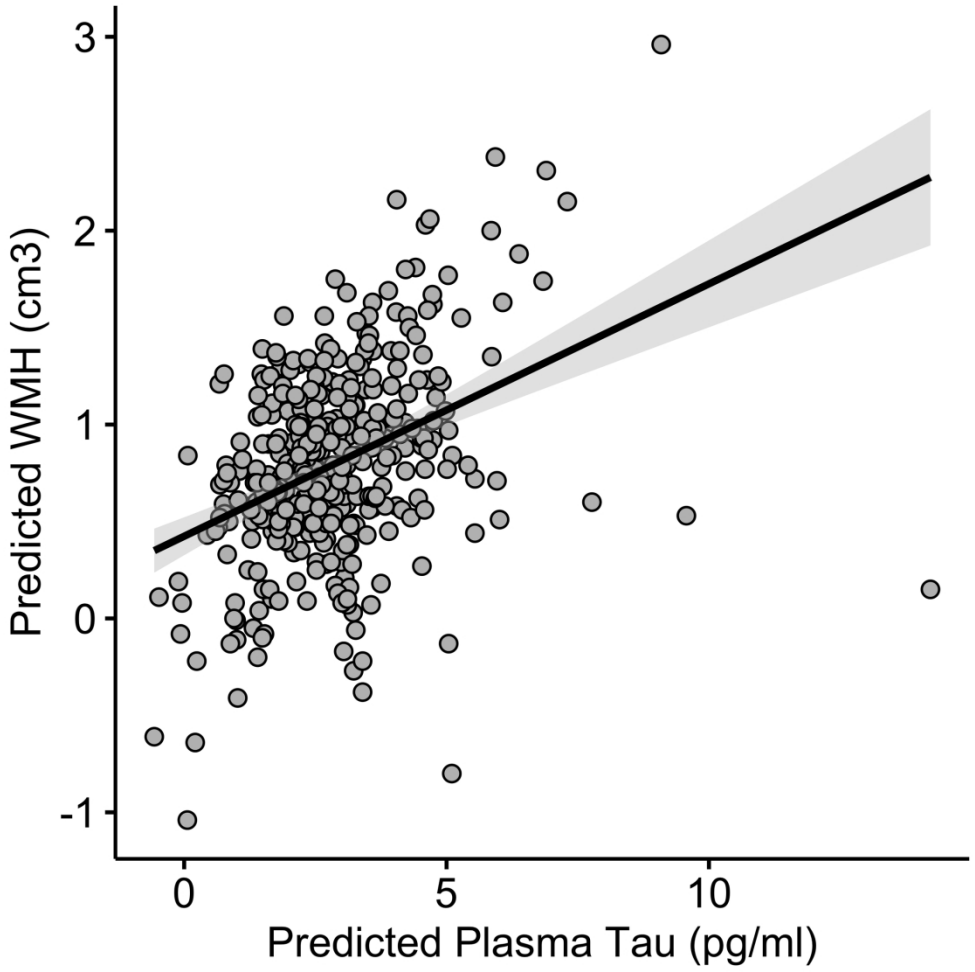

Figure 2. Linear association between white matter hyperintensities (WMH) and plasma tau. Main effect of predicted WMH plotted against predicted plasma tau values obtained from the primary mixed design general linear model ($F(1,382)=5.27$, $p=0.022$, $r2 =0.153$, $\beta=0.743$ (95% CI: 0.259-1.228)).

101x101mm (600 x 600 DPI)

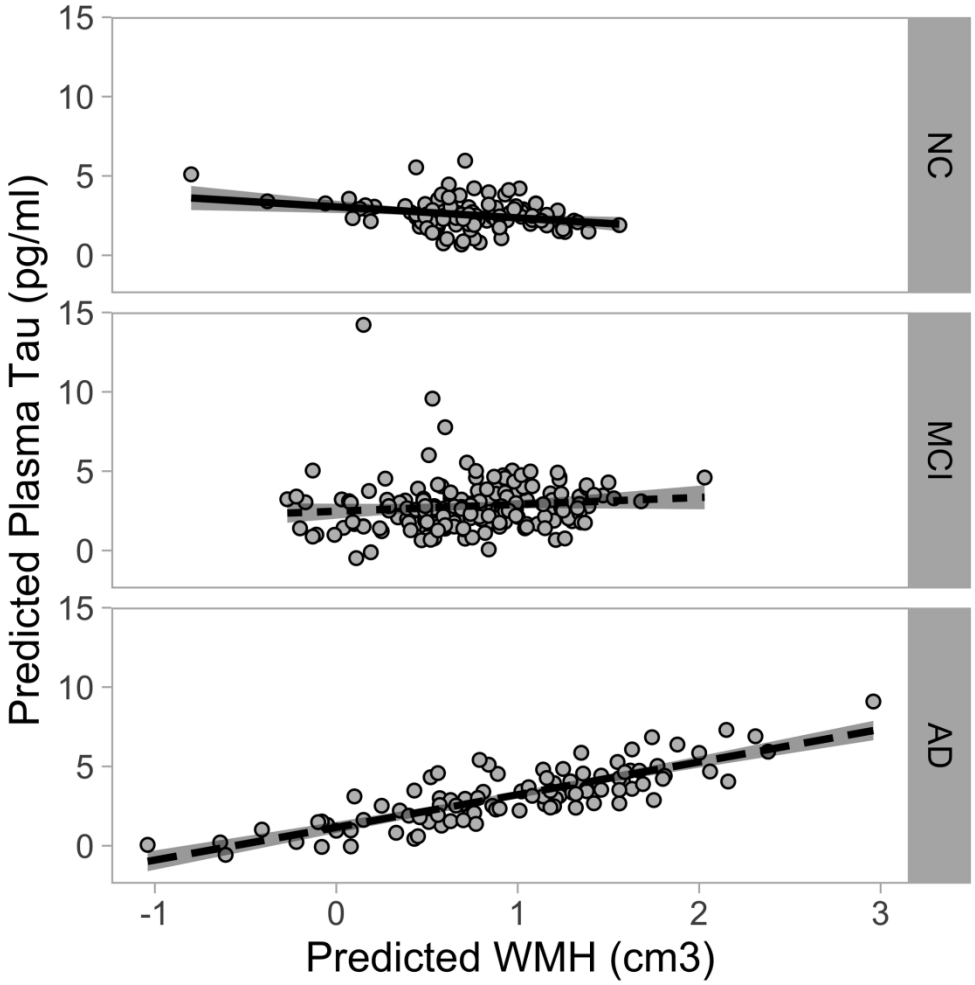

Figure 3. Interaction of WMH and plasma tau levels across diagnostic groups. Stratification across diagnostic groups demonstrate interactions between white matter hyperintensities and plasma tau burden at different diagnostic stages. Participants with Alzheimer's disease had the strongest association (NC: β=-0.083 (95% CI:-0.340-0.175), MCI: β=0.038 (95% CI: -0.152-0.229), AD: r2=0.677, β=0.448 (95% CI: 0.168-0.728)).

101x101mm (600 x 600 DPI)

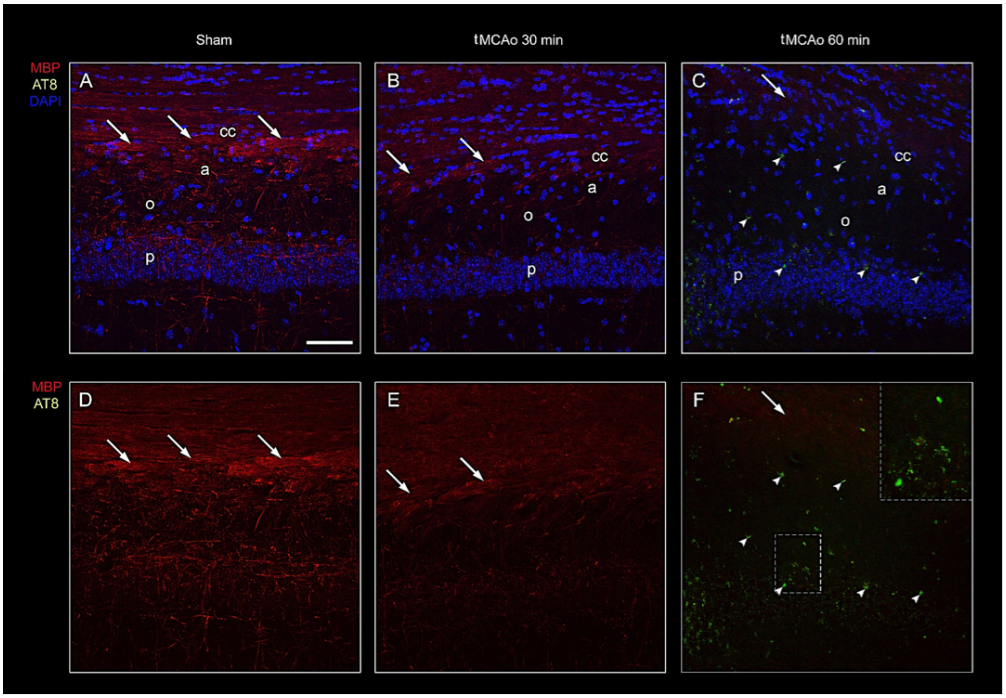

Figure 4. Transient middle cerebral artery occlusion (tMCAo) produces myelin basic protein (MBP) signal loss and induces tau phosphorylation. Representative microphotographs of MBP and AT8 immunofluorescence in mice without stroke (sham, A and D), tMCAo for 30 min (B and E) and 60 min (C and F). tMCAo produced a reduction of MBP (red signal; see arrows in C and F) and induced tau phosphorylation tau (AT8; green signal; see arrows in C, F and inset in F). The degree of ischemia-induced myelin loss and phosphorylation of tau increased with the increasing duration of ischemia (tMCAo) from 30 to 60 min. Panels A-C shows double immunofluorescence (MBP and AT8) with DAPI and panel D-F without DAPI. p, stratum pyramidal CA1; o, stratum oriens of CA1; a, alveus of CA1; corpus callosum. Scale bar = 50μm.

91x62mm (300 x 300 DPI)

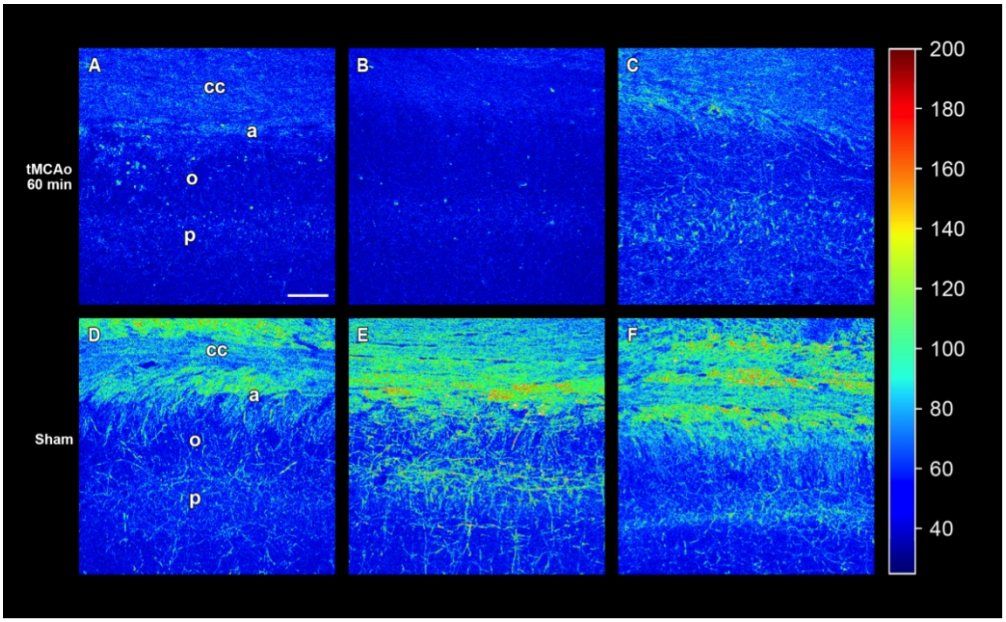

Figure 5. Mice subjected to transient middle cerebral artery occlusion (tMCAo) followed by 15 days reperfusion show strong alterations in the pattern and expression of myelin basic protein (MBP) in corpus callosum and CA1 region of the hippocampus. Shown are three examples of mice subjected to 60 min occlusion surgery (A-C;), which demonstrate a drastic change in MBP expression compared to sham surgery controls (D-F). In addition, tMCAo affects the MBP distribution pattern (compare A-C to D-F). These results suggest myelin loss and axonal damage due to ischemia-reperfusion that is still observed after 15 days. MBP colormap intensity pseudocolor-scale, red is the highest intensity and blue the lowest. cc, corpus callosum; a, alveus; o, stratum oriens; p, stratum pyramidale. Each panel represents an independent mouse (A-C; n=3 and D-F; n=3). Scale bar = 50μm.

100x61mm (300 x 300 DPI)

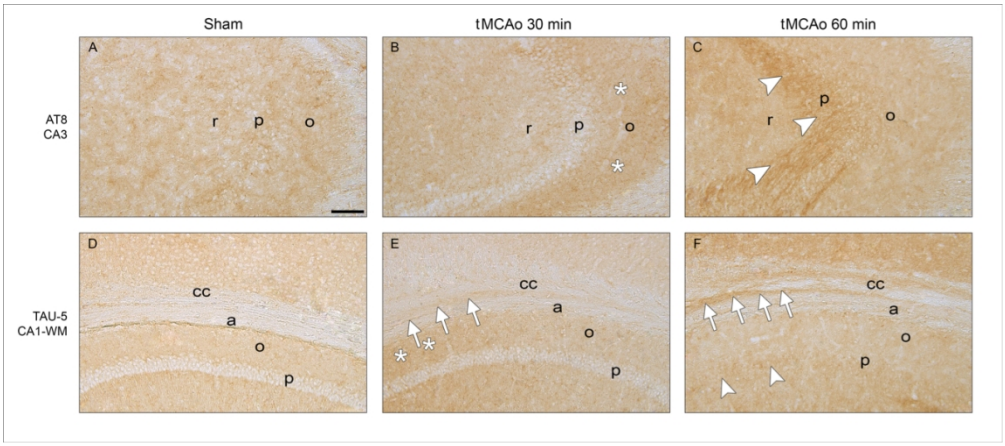

Figure 6. Mice undergoing transient middle cerebral artery occlusion (tMCAo) for thirty and sixty minutes followed by 15 days reperfusion exhibit higher total and phosphorylated tau immunostaining in the hippocampus and corpus callosum. Depicted here are representative images of total (Tau-5) and phosphorylated (AT8) tau immunostaining in the CA3 (A-C) and CA1 hippocampal subregions that includes white matter (alveus and corpus callosum areas) (D-F). Thirty minutes tMCAo produced a minor increase in Tau-5 and significant changes in AT8 staining in the stratum oriens (see asterisks in B and E) and corpus callosum (see arrows in E) compared to Sham (non-ischemia surgery A&D) control. Sixty minutes tMCAo showed a greater increase of phosphorylated tau (AT8) immunostaining in pyramidal cells layer of CA3 (arrowheads in C) in addition to significant high intensity of total tau (Tau-5) in the CA1 pyramidal cell layer and in the corpus callosum (see arrowheads and arrows in F). WM, white matter; p, stratum pyramidale; o, stratum oriens; r, stratum radiatum; a, alveus; cc; corpus callosum. Scale bar = 100μm.

114x50mm (300 x 300 DPI)

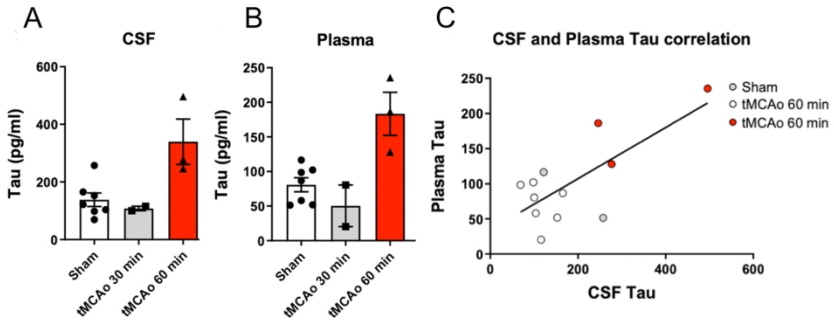

Figure 7. Cerebrospinal fluid and plasma tau concentrations differ between mice exposed to tMCAo and sham controls.

A CSF and B plasma tau concentrations were particularly pronounced for 60 min tMCAo ($F(2,11)=7.38$, $p=0.013$ and $F(2,11)=10.70$, $p=0.004$, respectively). Data are expressed as mean ± S.E.M. C Plasma and CSF values were strongly correlated ($R2=0.522$, $\beta=0.36$, $p=0.008$). n = 7 (Sham), n=2 (tMCAo 30 min), and n=3 (tMCAo 60 min). 60 minute condition displayed in red, 30 minute condition displayed in grey, and sham controls in white.

127x177mm (300 x 300 DPI)

Tables

Table 1. Demographic characteristics, amyloid status, and plasma tau levels for participants included in the study.

	NC	MCI	AD	Total	Statistic
N	108	186	97	391	- -
Age, mean (SD) years	75.17 (5.28)	73.88 (7.51)	74.75 (7.84)	74.45 (7.06)	F=1.25, p=0.288
Sex, n (%) women	54 (50.0%)	60 (32.3%)	42 (43.3%)	156 (39.3%)	X^2=9.59, p<0.008
Amyloid positive, n (%)	40 (37%)	136 (73%)	90 (92%)	266 (68%)	X^2=77.2, p<0.001
Plasma tau, mean (SD) pg	2.55 (1.33)	2.80 (1.72)	3.17 (1.36)	2.82 (1.55)	F=4.17, p=0.016

AD = clinical Alzheimer's disease; MCI = Mild Cognitive Impairment; NC = Cognitively Normal Controls

Table 2. Results of a series of logistic regression analyses that discriminate between clinical diagnostic groups based on amyloid, tau, white matter hyperintensity **(**WMH), and the interaction between WMH and tau.

	AD (1) vs. NC(0)			MCI (1) vs. NC (0)			AD (1) vs. MCI (0)		
Variable	B	Odds ratio (95% CI)	p-value	B	Odds ratio (95% CI)	p-value	B	Odds ratio (95% CI)	p-value
Age	<0.001	1.00 (0.949-1.054)	0.995	-0.036	0.965 (0.927-1.004)	0.077	0.016	1.016 (0.981-1.053)	0.369
Amyloid positivity	3.04	20.91 (8.68-50.39)	<0.001	1.59	4.894 (2.893-8.280)	<0.001	1.518	4.565 (1.944-10.721)	<0.001
Plasma tau	0.03	1.03 (0.741-1.434)	0.855	-0.073	0.930 (0.778-1.112)	0.427	0.036	1.036 (0.872-1.231)	0.684
WMH volume	-1.18	0.307 (0.104-0.907)	0.033	-0.619	0.538 (0.309-0.938)	0.029	-0.172	0.842 (0.504-1.409)	0.513
Plasma tau x WMH volume	0.49	1.624 (1.049-2.514)	0.030	0.239	1.270 (1.029-1.567)	0.026	0.066	1.068 (0.908-1.255)	0.426

A 95% Confidence Interval (CI) was reported for each interaction. AD = clinical Alzheimer's disease; MCI = Mild Cognitive Impairment; NC = Cognitively Normal Controls; WMH = White matter hyperintensity

Table 3. Demographic characteristics, Thal and Braak stages, and arteriosclerosis/atherosclerosis severity for autopsy cases included in the study.

		NC	MCI	AD	Total	Statistic
N		7	33	23	63	- -
Age, mean (SD) years		84.29 (6.78)	81.97 (6.15)	82.26 (8.73)	82.33 (7.18)	F= 0.30 p=0.745
Sex, n (%) women		2 (28.6%)	6 (18.2%)	6 (26.1%)	14 (22.2%)	X^2=0.67 p=0.714
Participants from Primary Analysis, n (%)		2 (7.4%)	17 (63.0%)	8 (29.6%)	27 (42.9%)	X^2=2.21 p=0.332
Thal Phase, n (%)	0-I	3 (42.9%)	5 (15.2%)	0 (0%)	8 (12.7%)	X^2=10.2 p=0.037
	II-III	1 (14.3%)	2 (6.1 %)	2 (8.7%)	5 (7.9%)	
	IIII - IV	3 (42.9%)	26 (78.8%)	21 (91.3%)	50 (79.4)	
Braak Stage, n (%)	0-I	2 (28.6%)	2 (6.1%)	0 (0%)	4 (6.3%)	X^2=15.1 p=0.019
	II-III	2 (28.6%)	9 (27.3%)	2 (8.7%)	13 (20.6%)	
	IV-V	3 (42.9%)	20 (60.6%)	15 (65.2%)	38 (60.3%)	
	VI	0 (0%)	2 (6.1%)	6 (26.1%)	8 (12.7%)	
Arteriosclerosis/ Atherosclerosis Index, mean (SD)		10.86 (6.26)	14.00 (6.86)	15.43 (7.66)	14.17 (7.12)	F= 1.13 p=0.329
NIA-AA AD Neuropathologic Score n, (%)	Not AD	2 (28.6%)	1 (3.0%)	0 (0%)	3 (4.8%)	X^2=19.3 p=0.013
	Low	1 (14.3 %)	10 (30.3%)	2 (8.7%)	13 (20.6%)	
	Intermediate	1 (14.3%)	2 (6.1%)	0 (0%)	3 (4.8%)	
	High	3 (42.9%)	19 (57.6%)	21 (91.3%)	43 (68.3%)	

AD = Alzheimer's disease; MCI = Mild Cognitive Impairment; NC = Cognitively Normal Controls NIA-AA = National Institute on Aging-Alzheimer's Association

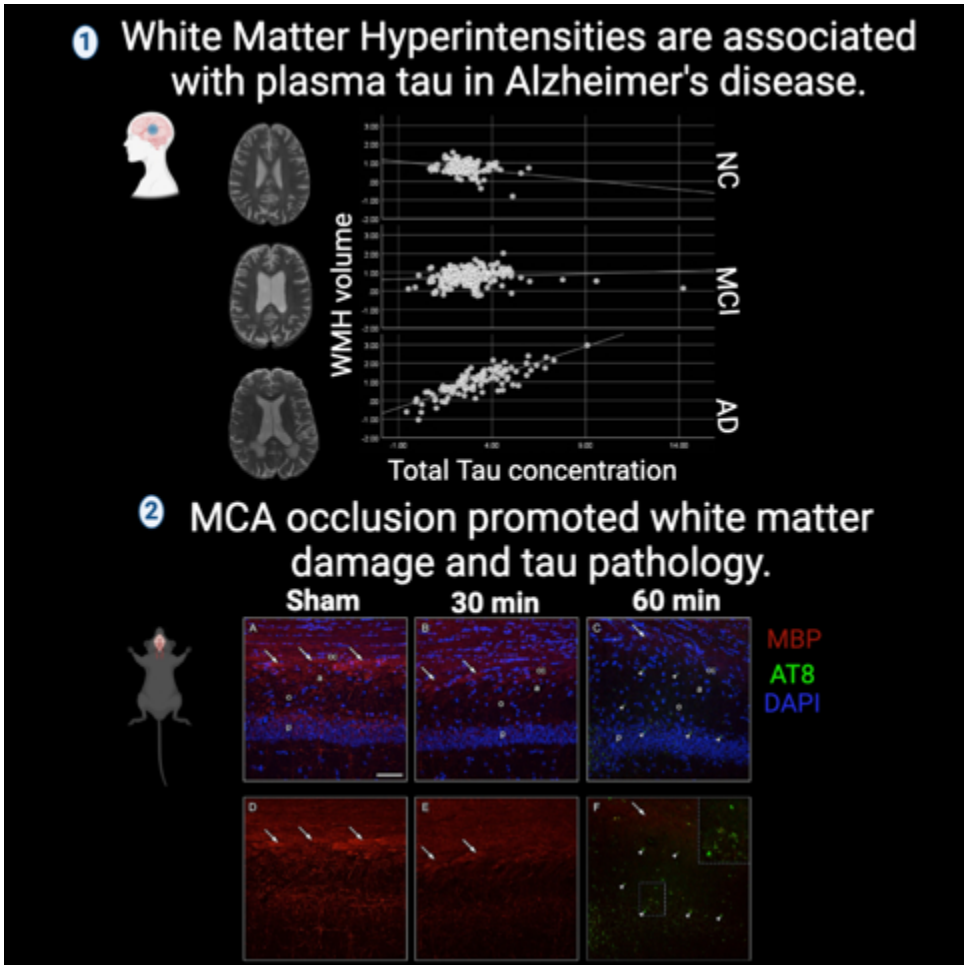

Graphical abstract

Abbreviated summary

Plasma-derived total-tau concentration is highly correlated with white matter hyperintensity volume, an MRI marker of small vessel ischemic damage, particularly among individuals with clinical Alzheimer's disease. A parallel mouse model confirmed white matter damage, hyperphosphorylated tau pathology, and elevated tau concentration in plasma and cerebrospinal fluid due to surgically induced ischemic injury.